ACS MATERIALS Au
AN OPEN ACCESS JOURNAL OF THE AMERICAN CHEMICAL SOCIETY

pubs.acs.org/materialsau

Article

Eu^{2+} Doping Concentration-Induced Site-Selective Occupation and Photoluminescence Tuning in $KSrScSi_2O_7:Eu^{2+}$ Phosphor

Shunqi Lai,[▽] Ming Zhao,[▽] Yifei Zhao, Maxim S. Molokeev, and Zhiguo Xia*

Cite This: *ACS Mater. Au* 2022, 2, 374−380

Read Online

ACCESS | Metrics & More | Article Recommendations | Supporting Information

ABSTRACT: Regulation of Eu^{2+} dopants in different cation sites of solid-state materials is of great significance for designing multicolor phosphors for light-emitting diodes (LEDs). Herein, we report the selective occupation of Eu^{2+} for multiple cationic sites in $KSrScSi_2O_7$, and the tunable photoluminescence from blue to cyan is realized through Eu^{2+} doping concentration-dependent crystal-site engineering. Eu^{2+} preferably occupies the K and Sr sites in $KSrScSi_2O_7$ at a low doping concentration, resulting in a 440 nm blue emission. As the Eu^{2+} concentration increases, a new Eu^{2+} substitution pathway is triggered, that is, Eu^{2+} enters the Sc site, leading to the red-shifted emission spectra from 440 to 485 nm. The doping mechanism and photoluminescence properties are corroborated by structural analysis, optical spectroscopy study, and density functional theory calculations. The optical properties of the as-fabricated white LEDs are studied, which demonstrates that these phosphors can be applied to full-spectrum phosphor-converted LEDs. This study provides a new design strategy to guide the development of multicolor Eu^{2+}-doped oxide phosphors for lighting applications.

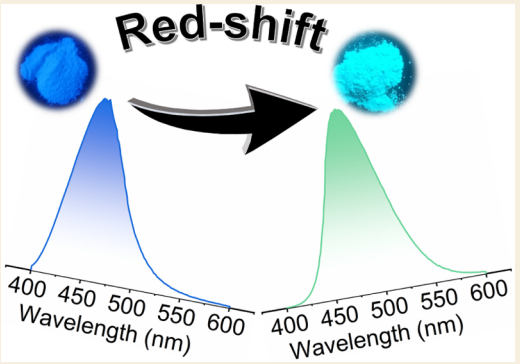

KEYWORDS: *photoluminescence, silicates, crystal-site engineering, doping, light-emitting diodes*

INTRODUCTION

Currently, healthy lighting with full spectrum and high quality has been favored in our daily life.[1] The fabrication of full-spectrum white light-emitting diodes (WLEDs) has become a research hot spot in the field of lighting due to their advantages not only to be close to the solar spectrum but also energy saving, high efficiency, and environmental friendliness.[2,3] Generally, traditional WLEDs are mainly obtained by combining a blue InGaN chip with the commercial yellow-emitting phosphor $Y_3Al_5O_{12}:Ce^{3+}$ (YAG:Ce).[4−7] Nevertheless, the absence of red spectral components would result in high-correlated color temperature (CCT > 5000 K) and poor color-rendering index (R_a < 80), which cannot meet the demands of healthy lighting.[8] In addition, the harsh blue light generated by blue light-emitting diode (LED) chips could hurt the endocrine system, human emotion, thoughtseize, and even the pace of life.[9] Hence, some researchers proposed to fabricate a lighting device using the phosphors of three primary colors combined with near-ultraviolet (n-UV) or ultraviolet (UV) chips that can diminish blue light and enable high-quality white light.[10−12] However, there still exists a cavity in the region of 480−520 nm compared with sunlight, which is called the "cyan gap".[13] This gap hinders the WLED devices from obtaining a true continuous white light spectrum similar to sunlight, and it also has a negative impact on the rhythm of life.[14,15] Consequently, it is very important to design a new kind of phosphor emitting in the blue-to-cyan spectral region to achieve full-spectrum lighting by cyan light compensation.[16−18]

As one of the most common and highly efficient activators, an Eu^{2+} ion possesses broadband absorption in the UV to blue regions (350−460 nm), as well as multicolor emission from 400 to 740 nm, originated from the highly efficient $4f^65d^1−4f^7$ parity-allowed electric dipole transition.[19,20] Furthermore, due to the exposed 5d electrons on the surface of Eu^{2+} ions, its energy state is susceptible to the local surroundings around the ion. Therefore, the multicolor emission can be achieved by intentionally controlling the local site symmetry, crystal field splitting, and the covalency between the activator and ligand.[21−25] In this regard, many strategies were put forward to regulate the site-selective occupation of Eu^{2+} and design the phosphor with the desired emission, such as modifying the synthetic route, neighboring cation/anion substitution, changing the doping concentration of Eu^{2+}, and so on.[26,27] Among them, changing the Eu^{2+} concentration has been served as an efficient way to regulate the local environment and site occupation of Eu^{2+} to harvest multicolor phosphors.[28] For

Received: December 22, 2021
Revised: February 9, 2022
Accepted: February 10, 2022
Published: February 24, 2022

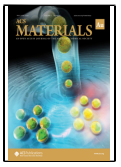

https://doi.org/10.1021/acsmaterialsau.1c00081
ACS Mater. Au 2022, 2, 374−380

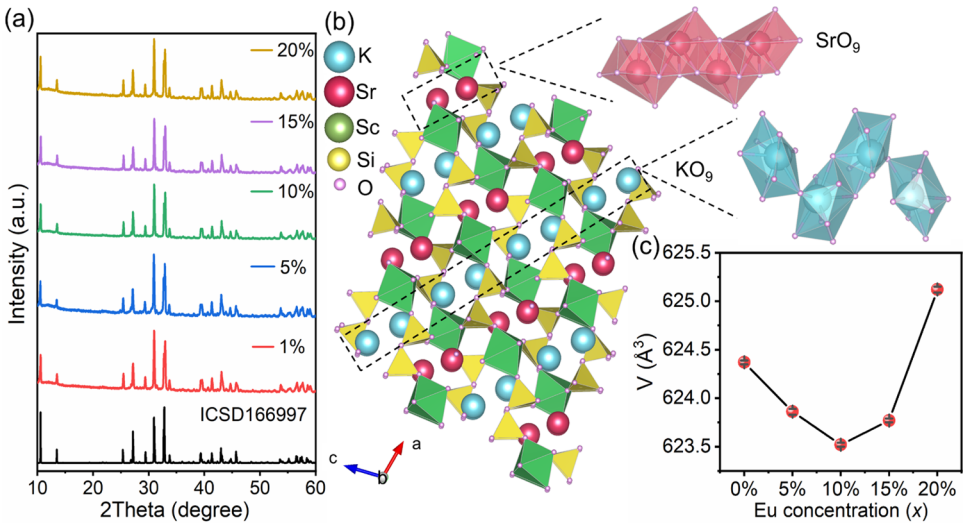

Figure 1. (a) XRD patterns of KSS:*x*Eu (x = 1−20%) and the theoretical pattern calculated on the base of ICSD card no.166997 as a reference. (b) Crystal structure of $KSrScSi_2O_7$. (c) Dependence of cell volume with the Eu concentration, and the nonlinear trend can be associated with different Eu occupation mechanisms.

example, Kakihana et al. successfully modulated the Eu^{2+} occupation site from Ca(1n) sites to Ca(2n) sites, which is smaller, to reach the tuning of photoluminescence from orange to red in $Ca_2SiO_4:Eu^{2+}$ by simply changing the Eu^{2+} concentration.[29] Tang studied the multicolor luminescence in $Li_2Sr_2Al(PO_4)_3:Eu^{2+}$ in the same way.[30] All of these systems have one specific feature in common, containing at least two cationic sites with different coordination environments.

In 2010, Maria reported a new scandium silicate compound $KSrScSi_2O_7$, which includes three different cationic sites (K, Sr, Sc) that may be occupied by Eu^{2+}.[31] Subsequently, Chen et al. doped Eu^{2+} ions into this host obtaining a blue-emitting phosphor, which was attributed to the Eu^{2+} ions locating in Sr sites.[32,33] As reported in $A_3BSi_2O_7$ (A refers to alkali metal ions and B stands for inert rare-earth ions), Eu^{2+} ions can occupy A and B sites, obtaining a stable system and bright emission.[34,35] Herein, taking the blue-emitting silicate phosphor $KSrScSi_2O_7:Eu^{2+}$ (KSS:Eu) as the research object, we intend to realize different occupations of Eu in KSS:Eu via changing the Eu^{2+} concentration to achieve the tunable emissions.

Accordingly, KSS:*x*Eu^{2+} phosphors dependent on different Eu^{2+} doping concentrations were synthesized, and the luminescence properties and mechanisms were studied in detail. At a low Eu^{2+} concentration, Eu^{2+} occupies K and Sr sites enabling blue emission; while increasing the concentration of Eu^{2+}, Eu^{2+} can be chemically driven to K and Sc sites, thereby achieving cyan emission. In this way, this cyan-emitting phosphor can be potentially used for full-spectrum lighting. This work reveals novel insights into the search for multicolor phosphors suitable for the full-spectrum LED illumination by Eu^{2+} site-selective occupation.

EXPERIMENTAL SECTION

Materials and Preparation

The designed samples of KSS:*x*Eu (x = 0−20%) were synthesized using the conventional high-temperature solid-state reaction method. Stoichiometric amounts of K_2CO_3 (A.R.), $SrCO_3$ (A.R.), SiO_2 (A.R.), Sc_2O_3 (A.R.), and Eu_2O_3 (99.99%) were mixed evenly by grounding them with ethanol for an appropriate time, and all of the chemicals were commercially purchased from Aladdin without further purification. First, the mixtures were sintered at 600 °C for 6 h under air and then sintered at 1150 °C for 4 h under a reducing atmosphere of 80%N_2−20%H_2. The final products were naturally cooled to room temperature (RT) and ground into fine powders for further measurement.

Characterization

X-ray diffraction (XRD) patterns were collected on an Aeris X-ray diffractometer (PANalytical Corporation, The Netherlands) operating at 40 kV and 15 mA with monochromatized Cu Kα radiation (λ = 1.5406 Å). Rietveld analyses of the powder XRD patterns were carried out by TOPAS 4.2 program.[36] Photoluminescence excitation (PLE) and emission (PL) spectra were recorded by an FLS1000 fluorescence spectrometer (Edinburgh Instruments Ltd., U.K.) equipped with a continuous 450 W xenon (Xe) lamp. The internal/external quantum efficiency (IQE/EQE) was checked using an integrated sphere on the same FLS1000 instrument. Temperature-dependent PL spectra were collected from 300 to 420 K using the FLS1000 with heating equipment. Decay curves were collected by the FLS1000 equipped with a 340 nm pulse diode, and the count number of photons is 5,000. All of the decay curves were fitted by FAST software supplied with the FLS1000.

LED Fabrication

WLED devices were fabricated based on n-UV chips (λ = 365 nm) encapsulated in epoxy resin containing selected phosphors. The photoelectric performance of the LEDs, namely, the emission spectra, luminous efficacy, CCT, R_a, and Commission Internationale de L'Eclairage (CIE) chromatic coordinates, were measured on an integrating sphere spectroradiometer system (ATA-1000, Everfine).

Computational Methodology

Density functional theory (DFT) calculations were implemented adopting the Vienna Ab initio Simulation Package (VASP).[37,38] The generalized gradient approximation (GGA) and Perdew−Burke−Ernzerhof (PBE) functionals were selected to represent the exchange−correlation interactions within the material systems.[39−41] For all of the calculations, the plane-wave basis cutoff energy was set to 400 eV. The 3 × 3 × 3 k-meshes centered on the Γ point were employed. The following convergence criteria were selected for the geometry optimizations: (1) the Hellmann−Feynman forces should not be greater than 0.05 eV/Å and (2) the total energy difference should be under 5×10^{-5} eV/atom. The formation energies are calculated based on a 2 × 3 × 2 $KScSrSi_2O_7$ supercell using the following equation

https://doi.org/10.1021/acsmaterialsau.1c00081
ACS Mater. Au 2022, 2, 374−380

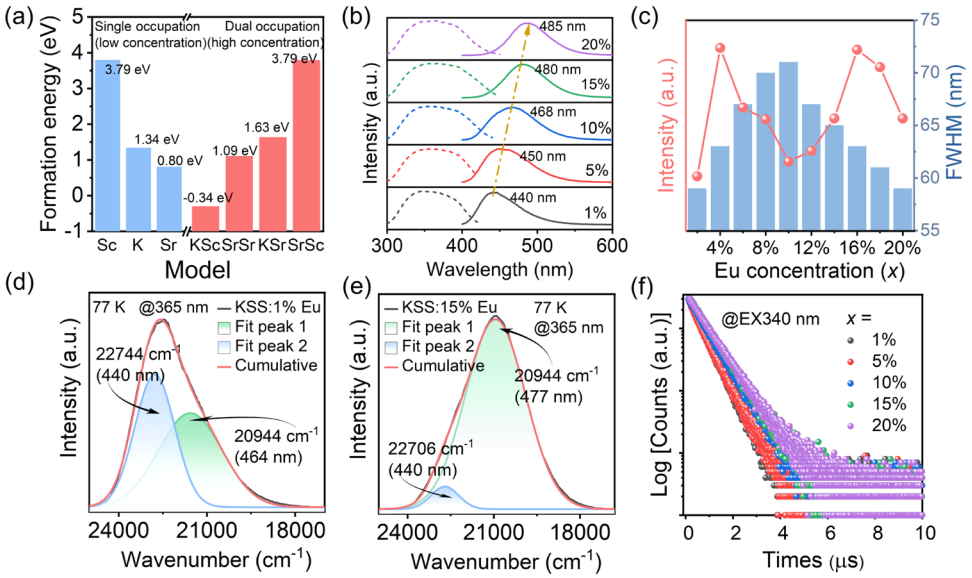

Figure 2. (a) Calculated formation energy for different variants of Eu substitution in $KSrScSi_2O_7$. (b) PLE (dotted line) and PL (solid line) spectra of KSS:Eu phosphors monitored at corresponding optimal wavelengths. (c) FWHM and the integrated intensity of KSS:Eu phosphors. The low-temperature emission spectra and Gaussian fitting results of (d) KSS:1%Eu and (e) KSS:15%Eu. (f) Decay curves of KSS:*x*Eu (x = 1−20%) at RT excited at 340 nm and monitored at the corresponding optimal emission wavelength.

$$E_f = E_{tot}\,(\text{defect}) - E_{tot}\,(\text{perfect}) - \sum_i n_i\mu_i \quad (1)$$

where E_{tot} (perfect) and E_{tot} (defect) are the total energy of the cells before and after introducing the dopants; μ_i refers to the referenced chemical potential of atoms that are involved in the defect formation; and n_i stands for the corresponding number of atoms. Each μ_i is derived from the corresponding single substance in the conventional phase.

RESULTS AND DISCUSSION

As shown in Figure 1a, the XRD patterns of KSS:*x*Eu (x = 1−20%) with different Eu^{2+} doping concentrations are compared with the standard pattern of $KSrScSi_2O_7$ (ICSD card no.166997).[31] Almost all diffraction peaks can be well indexed by the monoclinic space system ($P2_1/n$), except for small peaks of Sc_2O_3 and $SrSiO_3$ impurities. The parameters resemble those in the $KSrScSi_2O_7$ phase, which proves that the KSS:Eu phosphors have been successfully synthesized. To further understand the local structure and substitution mechanism of Eu^{2+} ions, we performed Rietveld refinement for KSS:*x*Eu (x = 1−20%), as shown in Figure S1. All of the refinement results were sufficiently reliable for its low *R*-factors (Table S1). Moreover, Table S2 listed the isotropic displacement parameters and fractional atomic coordinates of the studied phases for comparison. Figure 1b shows the schematic illustration of a $KSrScSi_2O_7$ crystal structure. Based on the isolated Si_2O_7 groups, the basic framework of the $KSrScSi_2O_7$ structure is formed by connecting nine-coordinated Sr cations, nine-coordinated K cations, and six-coordinated Sc cations. Adjacent ScO_6 polyhedra are linked to Si_2O_7 groups by sharing oxide atoms, and the Si−Si connected linearly along the *c*-axis, which creates the ScO_6 polyhedra layers in the ab plane and forms a three-dimensional (3D) skeleton with K and Sr cations located in the voids.[31]

In the $KSrScSi_2O_7$ structure, theoretically, Eu^{2+} ions can be located in cation sites of K, Sr, and Sc. Table S3 lists the specific radius of cations with different coordination numbers. As shown in Figure 1c, while the Eu ion concentration x ranges from 0 to 10%, the cell volume decreases first as x increases, and this indicates that Eu^{2+} ions mainly occupy K and/or Sr sites because the ionic radii of Eu^{2+} are smaller than those of K^+ and Sr^{2+} with the same coordination number while larger than that of Sc^{3+}. However, with the continuous increase of x, the cell volume begins to increase, indicating that a new site occupation mechanism of Eu^{2+} emerged, which would also involve the substitution in Sc sites. Then, the DFT simulations were carried out to further investigate the preferential site occupation of Eu^{2+} upon different doping concentrations, and the results of each model are summarized in Figure 2a. Considering the complex scenarios involving extra defects for charge balances, we have attempted to treat the substitutions as neutral defects first. Within a low doping concentration (the single Eu dopant in $K_{48}Sr_{48}Sc_{48}Si_{96}O_{336}$, giving an Eu molar ratio of 2%), Eu prefers to enter Sr and K sites, according to the relatively low formation energies. While provided with a higher Eu dosage (such as dual Eu substitution in the same pristine lattice, leading to Eu% = 4 mol %), Eu^{2+} ions became more likely to occupy K and Sc sites instead. Also, if the charge balances (e.g., oxygen defect) are included for the naturally charge-imbalanced models, the differences in formation energies would only be larger. Therefore, these DFT simulations could also suggest the concentration-dependent Eu^{2+} site preference from a theoretical perspective.

Figure 2b shows the PL and PLE spectra of KSS:*x*Eu^{2+} (x = 1−20%) at RT. The f−d transition of Eu^{2+} ions produces a broad excitation band ranging from 300 to 420 nm, and its peak position is almost unchanged with increasing Eu^{2+} concentration, besides slight increasing of bandwidth. As the Eu^{2+} concentration increases, the PL spectra excited at 365 nm present a continuous red shift from 440 blue light to 485 nm cyan light. To analyze the changing trend of emission spectra with the increase of the Eu^{2+} concentration in higher accuracy, we reduced the concentration step from 5 to 2%. As shown in Figure 2c, as x increases, the PL intensity experiences increases and decreases twice, and the full width at half-maximum (FWHM) increases first and then reduces. It is obvious that

https://doi.org/10.1021/acsmaterialsau.1c00081
ACS Mater. Au 2022, 2, 374−380

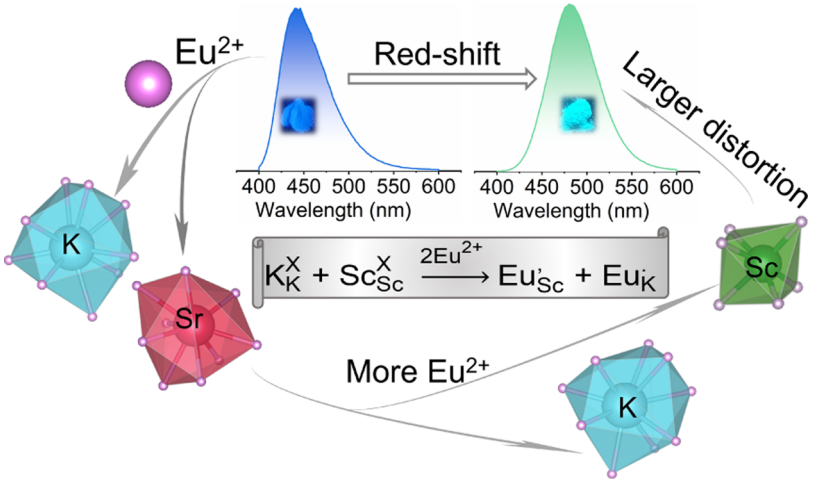

Figure 3. Schematic diagram of the optical tuning mechanism of KSS:Eu.

the point with the weakest PL intensity corresponds to the widest FWHM. We further tested the quantum yield (IQE and EQE), as shown in Table S4, and its variation was consistent with that of the luminescence intensity. All of those are related to the different Eu^{2+} occupation mechanisms, which will be discussed later.

The connection of the luminescent centers and the crystallographic positions in the crystal structure was further confirmed by measuring low-temperature spectra. The PL spectra of two selected samples of KSS:1%Eu and KSS:15%Eu at 77 K are depicted in Figure 2d,e, respectively. It can be seen that two Gaussian peaks can be well fitted to the spectral profile. Using the empirical eq 2 proposed by Van Uitert, we estimated the d-band-edge position of Eu^{2+} (E) to analyze the origin of the PL peaks[42]

$$E = Q\left[1 - \left(\frac{V}{4}\right)^{1/V} 10^{-nE_a r/80}\right] \quad (2)$$

where Q is 34 000 cm^{-1} (the d-band-edge position of Eu^{2+} free ions) and V is 2 (the valence of Eu^{2+}). E_a is the electron affinity of the anion, regarded as a constant here, n stands for the coordination number of Eu^{2+}, and r represents the substituted ion radius in the host. That is, E (cm^{-1}) is proportional to n and r. As n = 9 for the Sr and K sites, n = 6 for the Sc site, and r (K) > r (Sr) > r (Sc), the peak at 433 nm (435 nm) can be assigned to Eu^{2+} at the K site, the peak at 455 nm can be assigned to Eu^{2+} at the Sr site, and the peak at 481 nm can be assigned to Eu^{2+} at the Sc site.

Combined with the above structural analysis and DFT calculation results, it can be concluded that Eu^{2+} preferentially occupies Sr and K sites when the Eu^{2+} doping concentration is low. The optimal concentration is x = 4%, and the intensity of the emission spectrum starts to decrease when x is higher than 4%, resulting from the concentration quenching effect. As the Eu^{2+} concentration increases continuously, Eu^{2+} prefers to enter K and Sc sites, and it would lead to the continuous change of FWHM and the emission intensity, as shown in Figure 2c. The Sc site is a new site that can be occupied by Eu^{2+}, and the luminescence intensity of Eu^{2+} at the Sc site increases first and then decreases with increasing Eu^{2+} doping concentration. Figure 3 shows the schematic diagram of the luminescence mechanism changing with the Eu^{2+} concentration, and some detailed description will also be given later.

To further evaluate the PL properties, the decay curves of KSS:xEu phosphors with different concentrations monitored at the corresponding optimal emission wavelength and excited at 340 nm were also measured (Figure 2f). The single exponential function (3) listed below is used to fit the decay curves[43]

$$I = A \exp(-t/\tau) \quad (3)$$

In the function, A is a constant, τ stands for the decay time, and I corresponds to the luminescence intensity at time t. As can be seen from Table S5, the decay time increases gradually with increasing Eu^{2+} concentration. Normally, the lifetime would monotonously decrease with increasing Eu^{2+} concentration due to the increase of self-absorption rate and nonradiative energy transfer among Eu^{2+} ions. While the lifetime increases with the increase of Eu^{2+} concentration, it could be related to the change of the luminescence center because the decay behaviors would change with the local environment of Eu^{2+}. Comparing the decay times of phosphors for a certain excitation wavelength, different emission wavelengths can be used to demonstrate the presence of multiple Eu^{2+} luminescence centers. The lifetime of the luminescence varies greatly due to the influence of additional nonradiative contributions on the decay process as the luminescence center changes. Hence, the decay curves of KSS:1%Eu were monitored at different emission wavelengths (Figure S2 and Table S6). The lifetime curves of different monitored emission wavelengths show different decay trends. When the monitoring wavelengths are in the range of 400−460 nm, they are double exponential decay, while when the monitoring wavelengths are in the range of 470−500 nm, they are single exponential decay. The difference is due to the lifetime of the single luminescence center corresponding to monoexponential decay, while in the area where the luminescence peaks corresponding to different luminescence centers coincide, the lifetime is affected by multiple luminescence centers and presents multiexponential decay. In Figure 4a, the lifetime values are fitted as a function of the monitoring wavelength. Some significant differences in decay times can be easily observed, suggesting that there are different luminescence centers in KSS:1%Eu, and it corresponds to the result that Eu^{2+} occupies both K and Sr sites at a low concentration. Furthermore, the decay curves of KSS:15% Eu^{2+} recorded at different wavelengths are depicted in Figures S3 and 3b, and the fitting result is listed in Table S7. The

https://doi.org/10.1021/acsmaterialsau.1c00081
ACS Mater. Au 2022, 2, 374−380

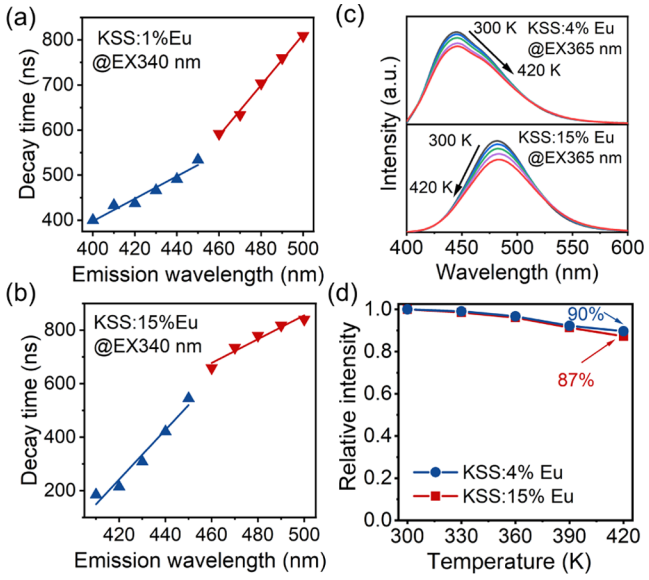

Figure 4. (a) Dependence of the KSS:1%Eu lifetime value on monitoring wavelength in the range of λ_{em} = 400−500 nm. (b) Dependence of the KSS:15%Eu lifetime value on monitoring wavelength in the range of λ_{em} = 410−500 nm. (c) PL spectra measured at different temperatures. (d) Dependence of temperature with an integrated emission intensity of KSS:4%Eu and KSS:15%Eu ranging from 300 to 420 K excited at 365 nm.

lifetimes also change greatly, verifying the two different luminescence centers (Eu_K and Eu_{Sc}), as also given in Figure 3.

The temperature quenching performance of KSS:*x*Eu powders were also investigated, which is one of the key parameters for evaluating a new type of WLED phosphor. Upon the excitation with the UV light of 365 nm, the temperature-dependent emission spectra of KSS:4%Eu and KSS:15%Eu at 300−420 K are shown in Figure 3e. Due to the increased probability of nonradiative transition, they both decrease slowly with increasing temperature. It can be seen from Figure 3f that at 420 K, the integrated intensity of KSS:4%Eu is 90% of that at RT, and the integrated intensity of KSS:15%Eu is 87% of that at RT, both of which are suitable for WLED device applications.

To further assess the application prospects of KSS:Eu in WLEDs, we fabricated the WLED lamp (LED 1) using the blue-emitting KSS:4%Eu, commercial green-emitting $(Sr,Ba)_2SiO_4:Eu^{2+}$ phosphor, and commercial red-emitting $Sr_2Si_5N_8:Eu^{2+}$ phosphor on an n-UV LED chip (λ = 365 nm). LED 1 shows warm white light with a CIE chromaticity coordinate of (0.3644, 0.3762), CCT as 4458 K, and R_a as 88.2 under 20 mA drive current. As shown in Figure 5a, due to the cyan gap, the R_a value of the LED 1 device is limited, which is difficult to exceed 90. However, after adding the cyan-emitting KSS:15%Eu phosphor to the device, LED 2 with a similar chromaticity coordinate (0.3626, 0.3581) and CCT (4566 K) can be obtained (Figure 5b). Meanwhile, the R_a can be improved obviously to 94.6, suggesting the high value of full-spectrum lighting. All of those demonstrate the great application prospects of these multicolor phosphors in high-quality full-spectrum lighting.

CONCLUSIONS

To sum up, we proposed a crystal-site engineering method to detect the Eu^{2+} luminescence in $KSrScSi_2O_7$ with diverse

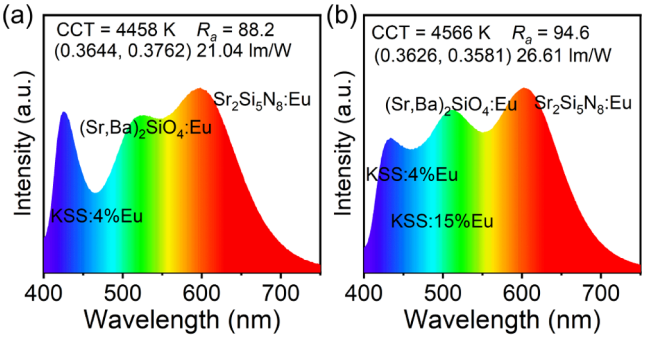

Figure 5. PL spectra of WLEDs fabricated using commercial phosphors $(Sr,Ba)_2SiO_4:Eu$ and $Sr_2Si_5N_8:Eu$ with (a) KSS:4%Eu or with (b) KSS:4%Eu and KSS:15%Eu on an n-UV LED chip (λ = 365 nm) under 20 mA drive current.

crystallographic sites. Photoluminescence tuning from blue to cyan was realized in KSS:Eu phosphors depending on Eu^{2+} doping concentrations. At low Eu^{2+} concentrations, Eu^{2+} prefers to occupy the K and Sr sites, whereas, with increasing Eu^{2+} concentration, Eu^{2+} can be chemically driven to the K and Sc sites to reach a more stable environment. The analysis of DFT calculation and decay curves further confirms the site-selective occupation mechanism. The fabricated WLED based on KSS:15%Eu, KSS:4%Eu, and commercial phosphors $(Sr,Ba)_2SiO_4:Eu^{2+}$ and $Sr_2Si_5N_8:Eu^{2+}$ shows a high R_a (94.6) and a low CCT (4566 K), indicating that the cyan-emitting KSS:15%Eu phosphor can be applied to high-quality pc-WLEDs in full-spectrum lighting. The design principle on the Eu^{2+} doping concentration-induced site-selective occupation provides a new gateway to find multicolor phosphors suitable for full-spectrum lighting applications.

ASSOCIATED CONTENT

Supporting Information

The Supporting Information is available free of charge at https://pubs.acs.org/doi/10.1021/acsmaterialsau.1c00081.

Rietveld refinement results (Figure S1, Tables S1−S3); PLQY (Table S4); and lifetimes (Figures S2 and S3, Tables S5−S7) (PDF)

AUTHOR INFORMATION

Corresponding Author

Zhiguo Xia − *State Key Laboratory of Luminescent Materials and Devices and Guangdong Provincial Key Laboratory of Fiber Laser Materials and Applied Techniques, School of Materials Science and Engineering, South China University of Technology, Guangzhou 510641, China*; orcid.org/0000-0002-9670-3223; Email: xiazg@scut.edu.cn

Authors

Shunqi Lai − *State Key Laboratory of Luminescent Materials and Devices and Guangdong Provincial Key Laboratory of Fiber Laser Materials and Applied Techniques, School of Materials Science and Engineering, South China University of Technology, Guangzhou 510641, China*

Ming Zhao − *Institute of Information Photonics Technology, Faculty of Science, Beijing University of Technology, Beijing 100124, China*

Yifei Zhao − *State Key Laboratory of Luminescent Materials and Devices and Guangdong Provincial Key Laboratory of*

https://doi.org/10.1021/acsmaterialsau.1c00081
ACS Mater. Au 2022, 2, 374−380

Fiber Laser Materials and Applied Techniques, School of Materials Science and Engineering, South China University of Technology, Guangzhou 510641, China; Department of Chemistry, City University of Hong Kong, Kowloon 999077 Hong Kong, China

Maxim S. Molokeev − *Laboratory of Crystal Physics, Kirensky Institute of Physics, Krasnoyarsk 660036, Russia; Research and Development Department, Kemerovo State University, Kemerovo 650000, Russia; Department of Physics, Far Eastern State Transport University, Khabarovsk 680021, Russia; Siberian Federal University, Krasnoyarsk 660041, Russia;* orcid.org/0000-0002-8297-0945

Complete contact information is available at: https://pubs.acs.org/10.1021/acsmaterialsau.1c00081

Author Contributions

[▽]S.L. and M.Z. contributed equally.

Notes

The authors declare no competing financial interest.

■ ACKNOWLEDGMENTS

This work was supported by the International Cooperation Project of National Key Research and Development Program of China (2021YFE0105700), the National Natural Science Foundations of China (Grant Nos. 51972118 and 51961145101), the Guangzhou Science & Technology Project (202007020005), the Local Innovative and Research Teams Project of Guangdong Pearl River Talents Program (2017BT01X137), and the China Postdoctoral Science Foundation (2021M700298). This work was also funded by RFBR according to research project No. 19-52-80003.

■ REFERENCES

(1) Xia, Z.; Liu, Q. Progress in discovery and structural design of color conversion phosphors for LEDs. *Prog. Mater. Sci.* **2016**, *84*, 59−117.

(2) Zhou, X.; Qiao, J.; Xia, Z. Learning from mineral structures toward new luminescence materials for light-emitting diode applications. *Chem. Mater.* **2021**, *33*, 1083−1098.

(3) Zhou, X.; Tian, P.; Sher, C.-W.; Wu, J.; Liu, H.; Liu, R.; Kuo, H.-C. Growth, transfer printing and colour conversion techniques towards full-colour micro-LED display. *Prog. Quantum Electron.* **2020**, *71*, No. 100263.

(4) Atuchin, V. V.; Beisel, N. F.; Galashov, E. N.; Mandrik, E. M.; Molokeev, M. S.; Yelisseyev, A. P.; Yusuf, A. A.; Xia, Z. Pressure-stimulated synthesis and luminescence properties of microcrystalline $(Lu,Y)_3Al_5O_{12}:Ce^{3+}$ garnet phosphors. *ACS Appl. Mater. Interfaces* **2015**, *7*, 26235−26243.

(5) Ji, H.; Wang, L.; Molokeev, M. S.; Hirosaki, N.; Xie, R.; Huang, Z.; Xia, Z.; ten Kate, O. M.; Liu, L.; Atuchin, V. V. Structure evolution and photoluminescence of $Lu_3(Al,Mg)_2(Al,Si)_3O_{12}:Ce^{3+}$ phosphors: new yellow-color converters for blue LED-driven solid state lighting. *J. Mater. Chem. C* **2016**, *4*, 6855−6863.

(6) Galashov, E. N.; Atuchin, V. V.; Gavrilova, T. A.; Korolkov, I. V.; Mandrik, Y. M.; Yelisseyev, A. P.; Xia, Z. Synthesis of $Y_3Al_5O_{12}:Ce^{3+}$ phosphor in the Y_2O_3−Al metal−CeO_2 ternary system. *J. Mater. Sci.* **2017**, *52*, 13033−13039.

(7) Meng, Q.; Zhao, G.; Zhu, Q.; Li, X.; Sun, X.; Li, J. G. Site-selective and cooperative doping of $Gd_3Al_5O_{12}$:Ce garnets for structural stabilization and warm WLED lighting of low CCT and high CRI. *Dalton Trans.* **2022**, *51*, 645−654.

(8) Zhang, Z.; Li, J.; Yang, N.; Liang, Q.; Xu, Y.; Fu, S.; Yan, J.; Zhou, J.; Shi, J.; Wu, M. A novel multi-center activated single-component white light-emitting phosphor for deep UV chip-based high color-rendering WLEDs. *Chem. Eng. J.* **2020**, *390*, No. 124601.

(9) Nagare, R.; Rea, M. S.; Plitnick, B.; Figueiro, M. G. Effect of white light devoid of "cyan" spectrum radiation on nighttime melatonin suppression over a 1-h exposure duration. *J. Biol. Rhythms* **2019**, *34*, 195−204.

(10) Xia, Z.; Zhang, Y.; Molokeev, M. S.; Atuchin, V. V. Structural and luminescence properties of yellow-emitting $NaScSi_2O_6:Eu^{2+}$ phosphors: Eu^{2+} site preference analysis and generation of red emission by codoping Mn^{2+} for white-light-emitting diode applications. *J. Phys. Chem. C* **2013**, *117*, 20847−20854.

(11) Ji, H.; Huang, Z.; Xia, Z.; Molokeev, M. S.; Atuchin, V. V.; Fang, M.; Huang, S. New yellow-emitting Whitlockite-type structure $Sr_{1.75}Ca_{1.25}(PO_4)_2:Eu^{2+}$ phosphor for near-UV pumped white light-emitting devices. *Inorg. Chem.* **2014**, *53*, 5129−5135.

(12) Liao, H.; Zhao, M.; Molokeev, M. S.; Liu, Q.; Xia, Z. Learning from a mineral structure toward an ultra-narrow-band blue-emitting silicate phosphor $RbNa_3(Li_3SiO_4)_4:Eu^{2+}$. *Angew. Chem., Int. Ed.* **2018**, *57*, 11728−11731.

(13) Zhong, J.; Zhuo, Y.; Hariyani, S.; Zhao, W.; Wen, J.; Brgoch, J. Closing the cyan gap toward full-spectrum LED lighting with $NaMgBO_3:Ce^{3+}$. *Chem. Mater.* **2020**, *32*, 882−888.

(14) Oh, J. H.; Yang, S. J.; Do, Y. R. Healthy, natural, efficient and tunable lighting: four-package white LEDs for optimizing the circadian effect, color quality and vision performance. *Light: Sci. Appl.* **2014**, *3*, No. e141.

(15) Pauley, S. M. Lighting for the human circadian clock: recent research indicates that lighting has become a public health issue. *Med. Hypotheses* **2004**, *63*, 588−596.

(16) Zhao, M.; Zhou, Y.; Molokeev, M. S.; Zhang, Q.; Liu, Q.; Xia, Z. Discovery of new narrowband phosphors with the UCr_4C_4 -related type structure by alkali cation effect. *Adv. Opt. Mater.* **2019**, *7*, No. 1801631.

(17) Zhang, X.; Zhang, J.; Wu, X.; Yu, L.; Liu, Y.; Xu, X.; Lian, S. Discovery of blue-emitting Eu^{2+}-activated sodium aluminate phosphor with high thermal stability via phase segregation. *Chem. Eng. J.* **2020**, *388*, No. 124289.

(18) Zhao, M.; Liao, H.; Molokeev, M. S.; Zhou, Y.; Zhang, Q.; Liu, Q.; Xia, Z. Emerging ultra-narrow-band cyan-emitting phosphor for white LEDs with enhanced color rendition. *Light: Sci. Appl.* **2019**, *8*, No. 38.

(19) Wei, Q.; Ding, J.; Chen, H.; Zhang, Q.; Wang, Y. A novel yellow-green emitting phosphor with hafnium silicon multiple rings structure for light-emitting diodes and field emission displays. *Chem. Eng. J.* **2020**, *385*, No. 123392.

(20) Qin, X.; Liu, X.; Huang, W.; Bettinelli, M.; Liu, X. Lanthanide-activated phosphors based on 4f-5d optical transitions: theoretical and experimental aspects. *Chem. Rev.* **2017**, *117*, 4488−4527.

(21) Xia, Z.; Poeppelmeier, K. R. Chemistry-inspired adaptable framework structures. *Acc. Chem. Res.* **2017**, *50*, 1222−1230.

(22) Hu, T.; Gao, Y.; Molokeev, M. S.; Xia, Z.; Zhang, Q. Eu^{2+} stabilized at octahedrally coordinated Ln^{3+} site enabling red emission in $Sr_3LnAl_2O_{7.5}$ (Ln = Y or Lu) phosphors. *Adv. Opt. Mater.* **2021**, *9*, No. 2100077.

(23) Ji, H.; Huang, Z.; Xia, Z.; Molokeev, M. S.; Atuchin, V. V.; Huang, S. Cation substitution dependent bimodal photoluminescence in whitlockite structural $Ca_{3-x}Sr_x(PO_4)_2:Eu^{2+}$ ($0 \le x \le 2$) solid solution phosphors. *Inorg. Chem.* **2014**, *53*, 11119−11124.

(24) Wang, Z.; Xia, Z.; Molokeev, M. S.; Atuchin, V. V.; Liu, Q. Blue-shift of Eu^{2+} emission in $(Ba,Sr)_3Lu(PO_4)_3:Eu^{2+}$ eulytite solid-solution phosphors resulting from release of neighbouring-cation-induced stress. *Dalton Trans.* **2014**, *43*, 16800−16804.

(25) Wei, Y.; Lin, C. C.; Quan, Z.; Molokeev, M. S.; Atuchin, V. V.; Chan, T.-S.; Liang, Y.; Lin, J.; Li, G. Structural evolution induced preferential occupancy of designated cation sites by Eu^{2+} in $M_5(Si_3O_9)_2$ (M = Sr, Ba, Y, Mn) phosphors. *RSC Adv.* **2016**, *6*, 57261−57265.

(26) Zhuo, Y.; Hariyani, S.; Zhong, J.; Brgoch, J. Creating a green-emitting phosphor through selective rare-Earth site preference in $NaBaB_9O_{15}$:Eu^{2+}. *Chem. Mater.* **2021**, *33*, 3304−3311.
(27) Xia, Z.; Liu, G.; Wen, J.; Mei, Z.; Balasubramanian, M.; Molokeev, M. S.; Peng, L.; Gu, L.; Miller, D. J.; Liu, Q.; Poeppelmeier, K. R. Tuning of photoluminescence by cation nanosegregation in the $(CaMg)_x(NaSc)_{1-x}Si_2O_6$ solid solution. *J. Am. Chem. Soc.* **2016**, *138*, 1158−1161.
(28) Qiao, J.; Zhou, Y.; Molokeev, M. S.; Zhang, Q.; Xia, Z. Narrow bandwidth luminescence in $Sr_2Li(Al,Ga)O_4$:Eu^{2+} by selective site occupancy engineering for high definition displays. *Laser Photonics Rev.* **2021**, *15*, No. 2100392.
(29) Sato, Y.; Kato, H.; Kobayashi, M.; Masaki, T.; Yoon, D. H.; Kakihana, M. Tailoring of deep-red luminescence in Ca_2SiO_4:Eu^{2+}. *Angew. Chem., Int. Ed.* **2014**, *53*, 7756−7759.
(30) Wanjun, T.; Zhengxi, H.; Jiaxuan, L. Controllable luminescence in Eu^{2+}-doped $Li_2Sr_2Al(PO_4)_3$ phosphor via tuning the Eu^{2+} concentration and codoping Ce^{3+}. *J. Alloys Compd.* **2019**, *778*, 612−617.
(31) Wierzbicka-Wieczorek, M.; Kolitsch, U.; Tillmanns, E. The crystal structures of three new complex silicates of scandium. *Can. Mineral.* **2010**, *48*, 51−68.
(32) Chouhan, V. R.; Malviya, N.; Tadge, P.; Ray, S. Preparation characterization and luminescence investigations of Eu^{2+} activated scandium based phosphor ($KSrScSi_2O_7$ and $NaBaScSi_2O_7$) by AMC method. *J. Chem. Chem. Sci.* **2016**, *6*, 449−457.
(33) Ray, S.; Fang, Y.-C.; Chen, T.-M. $KSrScSi_2O_7$:Eu^{2+}: a novel near-UV converting blue-emitting phosphor with high efficiency and excellent thermal stability. *RSC Adv.* **2013**, *3*, 16387−16391.
(34) Qiao, J.; Ning, L.; Molokeev, M. S.; Chuang, Y. C.; Zhang, Q.; Poeppelmeier, K. R.; Xia, Z. Site-selective occupancy of Eu^{2+} toward blue-light-excited red emission in a $Rb_3YSi_2O_7$:Eu phosphor. *Angew. Chem., Int. Ed.* **2019**, *58*, 11521−11526.
(35) Qiao, J.; Amachraa, M.; Molokeev, M.; Chuang, Y.-C.; Ong, S. P.; Zhang, Q.; Xia, Z. Engineering of $K_3YSi_2O_7$ to tune photoluminescence with selected activators and site occupancy. *Chem. Mater.* **2019**, *31*, 7770−7778.
(36) *Bruker AXS TOPAS V4. In General profile and structure analysis software for powder diffraction data. − User's Manual*; Kalsruhe: Germany, 2008.
(37) Kresse, G.; Furthmüller, J. Efficiency of ab-initio total energy calculations for metals and semiconductors using a plane-wave basis set. *Comp. Mater. Sci.* **1996**, *6*, 15−50.
(38) Kresse, G.; Furthmüller, J. Efficient iterative schemes for ab initio total-energy calculations using a plane-wave basis set. *Phys. Rev. B* **1996**, *54*, 11169−11186.
(39) Hasnip, P. J.; Pickard, C. J. Electronic energy minimisation with ultrasoft pseudopotentials. *Comput. Phys. Commun.* **2006**, *174*, 24−29.
(40) Perdew, J. P.; Chevary, J. A.; Vosko, S. H.; Jackson, K. A.; Pederson, M. R.; Singh, D. J.; Fiolhais, C. Atoms, molecules, solids, and surfaces: Applications of the generalized gradient approximation for exchange and correlation. *Phys. Rev. B* **1992**, *46*, 6671−6687.
(41) Perdew, J. P.; Burke, K.; Ernzerhof, M. Generalized gradient approximation made simple. *Phys. Rev. Lett.* **1996**, *77*, 3865−3868.
(42) Lever, A. B. P. The crystal field splitting parameter Dq: calculation and significance. *Adv. Chem.* **1967**, *62*, 430−451.
(43) Qiao, J.; Zhou, G.; Zhou, Y.; Zhang, Q.; Xia, Z. Divalent europium-doped near-infrared-emitting phosphor for light-emitting diodes. *Nat. Commun.* **2019**, *10*, No. 5267.

https://doi.org/10.1021/acsmaterialsau.1c00081
ACS Mater. Au 2022, 2, 374−380